Communications on Applied Nonlinear Analysis
ISSN: 1074-133X
Vol 32 No. 3s (2025)

Servo System Design for Precise Fin Tip Control in Launch Vehicles Using Electromechanical Actuators

Albert John Varghese[1], Anuj Gupta[2], Rejo Roy[3#]

[1, 2, 3] Electrical Engineering, Rungta College of Engineering and Technology, Bhilai

Email - [1]albert.varghese@rungta.ac.in, [2]ganuj68314@gmail.com

[#] Corresponding Author – [3]rejo.roy@rungta.ac.in

Article History:

Received: *26-09-2024*

Revised: *13-11-2024*

Accepted: *28-11-2024*

Abstract:

This study examines the development and performance of a servo mechanism for fin tip control (FTC) in a launch vehicle, aimed at accurately manipulating rocket fins to achieve efficient steering. The analysis involves both linear and nonlinear modelling of the electromechanical actuator (EMA)-based FTC system, with the goal of developing a compensation strategy based on closed-loop control requirements. These specifications target position control for roll stabilization of launch vehicle during the FTC phase. A compensation approach, incorporating a PID controller and a notch filter, is integrated to meet the system's performance criteria. Friction, particularly Coulomb friction and Stiction, is a critical factor in achieving high-precision control using the EMA. To tackle this, a friction model is developed, and system parameters are determined by reducing the discrepancy between the outputs of the plant and the model, eliminating the need for optimization. The closed-loop performance of the system is then assessed through MATLAB/SIMULINK simulations, demonstrating the ability to meet the desired performance criteria for precise fin tip control.

Keyword: FTC system; electromechanical actuator; Servo system; Launch Vehicle; PID controller; Pulse Width Modulator; compensator.

1. INTRODUCTION:

A Launch Vehicle (LV) is a rocket-powered craft designed to transport payloads, such as spacecraft or satellites, from Earth's surface or lower atmosphere into space. These vehicles incorporate advanced aerodynamic designs and technologies, which, while improving performance, also result in high operational costs. The stability of a launch vehicle during flight is crucial for its trajectory control.

A few control system examples were considered to form a basic idea for designing a closed loop system help steer and stabilize the vehicle. The proposed system focuses on position control of the fins on a launch vehicle using electromechanical actuator and to handle the dynamics of the rocket fins and ensure precise roll control.

- Proportional Integral Derivative (PID) controlled Brushless DC (BLDC) motor speed system focuses on speed regulation in a closed-loop system, with the added complexity of temperature sensing. [1]

- To enhance efficiency, a Brain Emotional Logic-Based Intelligent Controller combined with an Advanced Hill Climb Search Maximum Power Point Tracking (MPPT) closed-loop control is simulated and optimized to address wind speed variations in a Wind Energy System. [2]
- An enhanced speed control approach for a BLDC motor drive system is proposed, focusing on optimizing motor speed regulation through the use of sensors and controllers, while ensuring the system remains efficient and cost-effective. The study explores MATLAB simulations for controlling speed under various load conditions. [3]
- A comparison of horizontal and vertical axis turbines using advanced control strategies like fuzzy logic controllers (FLC) and Hill Climb Search MPPT techniques to optimize power extraction under low wind speed conditions. It also involves MATLAB/Simulink simulations to evaluate the system's performance. [4]

Launch vehicles, or rockets, are equipped with movable fins located at the rear, which modify the aerodynamic forces acting on the vehicle. [5] In Figure 1, the trailing edge of the fin, shown in magenta, is deflected to the right, generating an aerodynamic force that causes the rocket's nose to move in that direction.

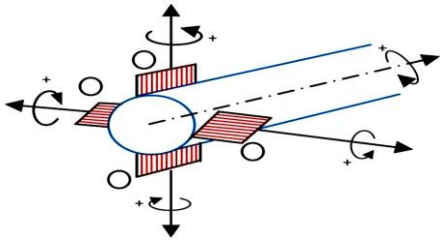

Fig. 1: Schematic for Fin control

The primary role of the fins is to provide stability during flight, helping the vehicle stay on its intended trajectory by generating rotational motion. This rotation is generated by the lifting forces produced by each fin. [6] The Fin Tip Control (FTC) and servo system control for the launch vehicle provides closed-loop position control for roll stabilization during the FTC phase. [7] Among the four fins, two are movable, and they are controlled by two independent electromechanical actuation systems, each powered by a brushless DC torque motor connected to a DC source. [8]

The actuator's deflection is measured using a potentiometer. The error signal is produced by comparing the position sensor's output with the input command. This error voltage is subsequently amplified, adjusted, and delivered to the redundant BLDC torque motor, which generates the necessary counteracting torque to nullify the error signal. [9] The control signal is amplified using a Pulse Width Modulated (PWM) amplifier. This document also includes the linear and nonlinear model parameters for the FTC system of the launch vehicle (LV), along with the corresponding test results.

2. MODELLING OF FTC SYSTEM:

The linear model of the FTC system is constructed through the following steps:

1. Creating a functional model.

2. Formulating the mathematical representation for each functional component through physical modelling.

3. Constructing the integrated linear model of the entire system.

2.1. FUNCTIONAL MODELLING

The FTC and servo system enable closed-loop position control for roll management of the launch vehicle during the FTC phase. This system employs an electromechanical actuator powered by a brushless torque motor driven by a DC source. Of the four fins in the setup, two are movable and controlled by the torque motor.

The compensation mechanism includes an analog position PID controller paired with an analog current loop. The torque motor coil is powered through a PWM-based power amplifier. A high-gain analog current loop around the PWM amplifier, operating within a bandwidth of a few kilohertz, guarantees the linear performance of the power amplifier.

A potentiometer is used to measure the angular position of the control surface, which is then compared to a voltage corresponding to the desired displacement (command input). The resulting error voltage is amplified, modified through a compensation scheme, and transmitted to the BLDC torque motor to produce the torque required to reduce the error signal. Power amplification of the control signal is achieved through a PWM amplifier.

2.2. PHYSICAL MODELLING

The mathematical representation of the system can be developed by combining the physical models of the various subsystems that constitute the system's linear framework. The physical model for the system is detailed in the subsequent sections.

2.2.1. Compensator Implementation Logic

The compensation scheme in the FTC system includes an analog position control mechanism. The torque motor is powered by a PWM-based amplifier that controls the current passing through the motor coil. A high-gain current loop maintains a stable current that matches the control voltage, effectively reducing nonlinearities in the PWM amplifier and compensating for variations in the power supply. [10]

The mechanical resonance between the equivalent stiffness and equivalent mass is determined based on fundamental principles, leading to the derivation of the resonance frequency as:

$$FrequencyResponse = \frac{1}{2\pi}\sqrt{\frac{{l_m}^2 * kl}{J_{eff}}} \qquad \text{---------- (1)}$$

Where, kl represents the equivalent stiffness of the mounting bracket, l_m is the length of the lever arm, and J_{eff} is the effective moment of inertia, which is calculated from the engine's moment of inertia J_{cs} and the motor rotor's moment of inertia J_m as shown below,

$$J_{eff} = \frac{J_{me} * J_{cs}}{J_{me} + J_{cs}} \qquad \text{---------- (2)}$$

Where, J_{me} is the reflected moment of inertia transferred from rotor to the engine side i.e., [11]

$$J_{me} = J_m * \left(\frac{lm}{nb}\right)^2 \quad \text{---------- (3)}$$

Where, nb is the ball screw ratio.

Here, $J_m = 11x10^{-4}$kg-m^2, $l_m = 0.0573$, $n_b = 6x10^{-3}/2/pi$ m/rad

So, $J_{me} = 0.0150$ (from eq. 3) and $J_{eff} = 0.3200$ (from eq. 2)

Frequency Resonance; $\omega_n = 343.122$ rad/sec or $f_n = 54.0488$ Hz

The mechanical resonance between the equivalent stiffness and equivalent mass is obtained from the linear model [12], and a notch filter is designed based on this information.

Notch filter transfer function,

$$Gn(s) = \frac{s^2 + 2\xi nn\omega_n s + {\omega_n}^2}{s^2 + 2\xi dn\omega_n s + {\omega_n}^2} \quad \text{---------- (4)}$$

Because, $\xi nn = 0.05$ & $\xi dn = 0.5$

$$Gn(s) = \frac{s^2 + 34.3122s + 117733}{s^2 + 343.122s + 117733} \quad \text{---------- (5)}$$

The analog position compensator (PID) [13] derived from the equation is as follows:

$$u(t) = Kc\left[e + \frac{1}{Ti}\int_0^t e(t)\,dt + Td\frac{de(t)}{dt}\right] \quad \text{---------- (6)}$$

$$U(s) = Kc\left[1 + \frac{1}{Tis} + Tds\right]E(s) \quad \text{---------- (7)}$$

Where, Td is derivative or rate time, and Ti is integral or reset time.

A PID controller consists of three tunable parameters: Kc, Ti, and Td. The derivative action predicts the error, enabling early corrective action and improving system stability. However, it does not directly influence the steady-state error. [14]

- When used alone, the derivative control mode cannot generate corrective effort for any constant error, regardless of its magnitude, which would result in an uncontrolled steady-state error. Therefore, derivative mode is not used in isolation and is always paired with another control mode to augment its functionality.
- The integral control mode eliminates steady-state offset in the controlled variable. However, it can significantly destabilize the system. This destabilizing effect is often mitigated by appropriately tuning the gain parameter Kc. [15]

The block diagram implementation of eq. 7 is sketched in Figure 2.

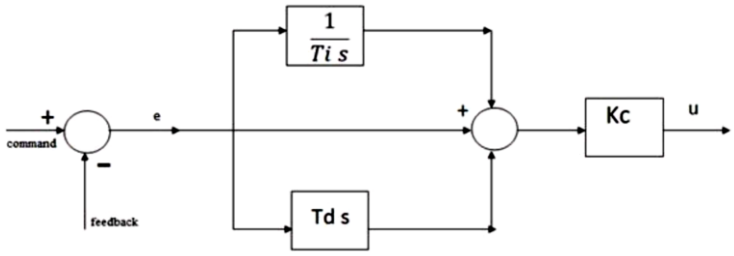

Fig. 2: Schematic representation of a PID controller

2.2.2. Functions of PID controller

Industrial controllers typically offer the following features for adjusting the output signal u(t) from a PID controller:

1. Tuning options for proportional, integral, and derivative control parameters. [16]
2. A direct/reverse action switch.
3. Adjustable limits on the control signal to prevent integral (reset) wind-up.

Effective tuning of the controller parameters, such as K_c and T_i, ensures satisfactory performance in many industrial processes. [17] In most cases, a small degree of oscillation, as shown in Figure 3, is considered acceptable.

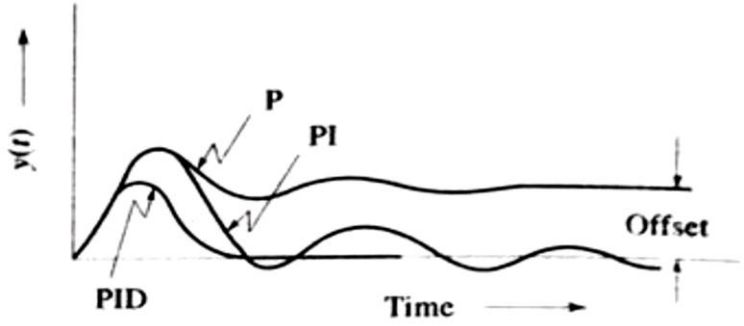

Fig. 3: Typical process response with feedback control

2.3. CURRENT LOOP MODELLING

The FTC system utilizes a brushless DC torque motor, with a ball screw mechanism that converts the motor's rotary motion into linear displacement to actuate the engine in the desired plane. The BLDC motor is controlled using a Hall sensor-based six-pulse commutation and a PWM power amplifier. A high-gain analog current loop with a bandwidth of a few kHz is used around the PWM amplifier to preserve the linear behavior of the power amplifier. Within the linear operating range of the power amplifier, the current through the torque motor coil (i_m) is expressed as:

$$i_m = V_i * K_A \quad \text{---------- (8)}$$

Figure 4 illustrates the functional block diagram of the FTC servo actuation system, offering an overview of the main components and their interactions.

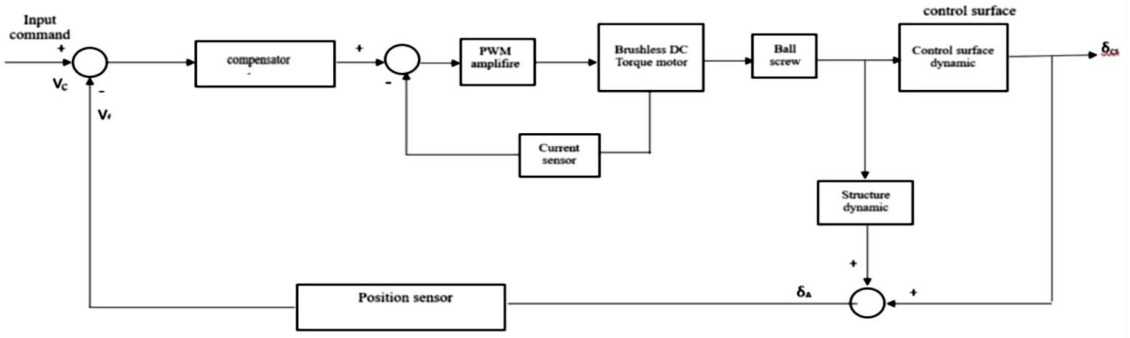

Fig. 4 Functional block diagram of FTC system

The linear and nonlinear equivalent models of the system are depicted in Figure 5 and Figure 6, respectively, highlighting the system's behaviour under different modelling assumptions.

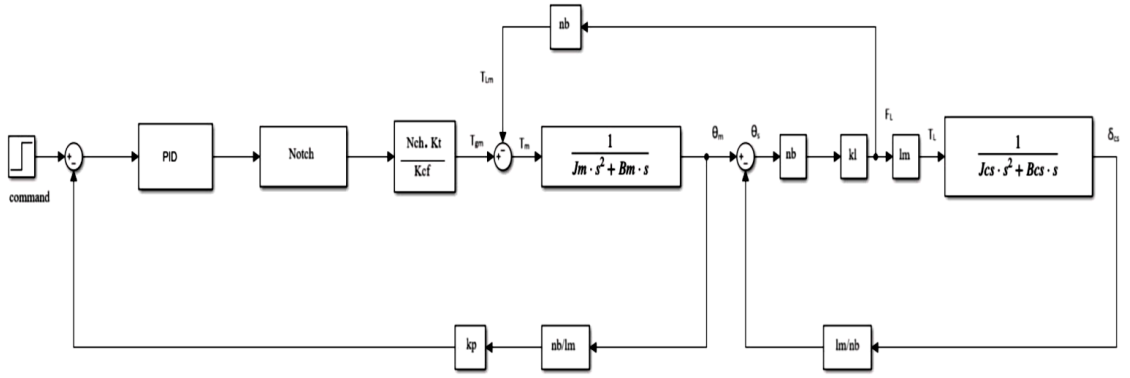

Fig.5 Linear model of FTC system

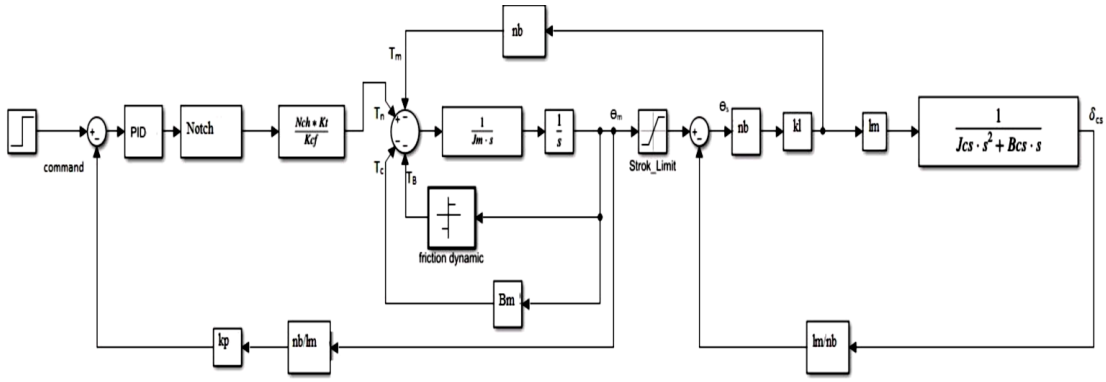

Fig.6 Nonlinear model of FTC system

Figure 7 demonstrates the compensation scheme employed in the FTC system, showcasing the control strategy used to enhance performance and stability.

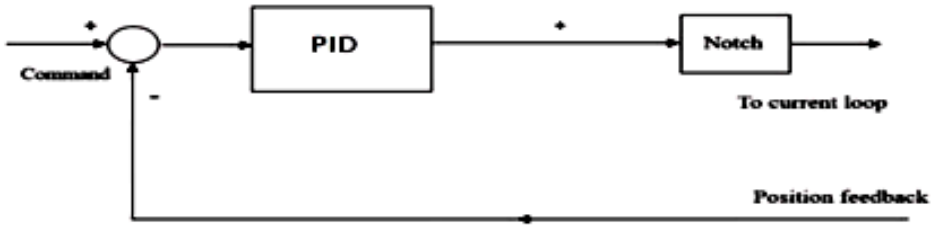

Fig.7 Compensation scheme of FTC system

2.4. FRICTION MODELLING

The friction in the motor arises from the ball screw used to convert rotary motion into linear motion. This friction is composed of two parts: stiction and Coulomb friction. Stiction force opposes rotor movement when the rotor is stationary or causes it to halt if the effective driving torque is less than the Coulomb friction. Running friction, or Coulomb friction (T_c), is a constant torque that resists the rotor's rotation when it is moving at a nonzero angular velocity.

$$Tc = TC.Sign(\omega_m) \quad \text{---------- (9)}$$

Where, TC is the magnitude of coulomb friction.

2.4.1. Stroke limit logic

The actuator's mechanical stroke is constrained to L1 during the push stroke and L2 during the pull stroke. If the actuator's output surpasses these limits, it is restricted to the maximum mechanical stroke. The motor's displacement is measured in terms of stroke, so the mechanical stroke limits are converted into equivalent motor deflection in radians and capped at the maximum allowable value.

For the push stroke, where L1 represents the mechanical limit (positive), the corresponding actuator rotation deflection is:

$$\theta_{lim1} = \frac{L1}{nb} \quad \text{---------- (10)}$$

If $\theta_m > \theta_{lim1}$, $\theta_m = \theta_{lim1}$ and $\omega_m = 0$

If L2 is the mechanical limit for the push stroke negative, the equivalent actuator rotation deflection is

$$\theta_{lim2} = \frac{L2}{nb} \quad \text{---------- (11)}$$

If $\theta_m > \theta_{lim2}$, $\theta_m = \theta_{lim2}$ and $\omega_m = 0$

Where, nb is Ball screw gear ratio (linear/rotary), θ_m is Motor angular position, L1 is Actuator stoke limit-Push, and L2 is Actuator stoke limit-Pull

2.4.2. Position Sensor Output

The actuator feedback is detected by a potentiometer, which measures the total actuator deflection, including both the fin deflection and the mounting structure deflection. [18] The scale factor for the servo loop command is given by:

$$Kp = \frac{10}{\delta_{csmax}} \qquad \text{---------- (12)}$$

Where, δ_{csmax} is the maximum control surface deflection.

The potentiometer scale factor is given by K_p potentiometer output, (V_f) is derived from the actuator position as follows;

$$Vf = \left(\theta m * \frac{nb}{lm}\right) * kp \qquad \text{---------- (13)}$$

3. SIMULATION RESULTS:

MATLAB/SIMULINK simulations are conducted for both linear and nonlinear models. Stability and performance are analyzed through open-loop and closed-loop frequency responses.

3.1. Simulation Setup

The linear and nonlinear models were simulated, and their stability responses are depicted in Figures 8 and 9. For the linear model, a PID controller and a notch filter were implemented in Simulink to achieve compensation, with the resulting stability response analyzed. In contrast, the nonlinear model incorporates stroke limit and friction dynamics as primary sources of nonlinearity, capturing a more realistic representation of the system's behaviour under practical conditions.

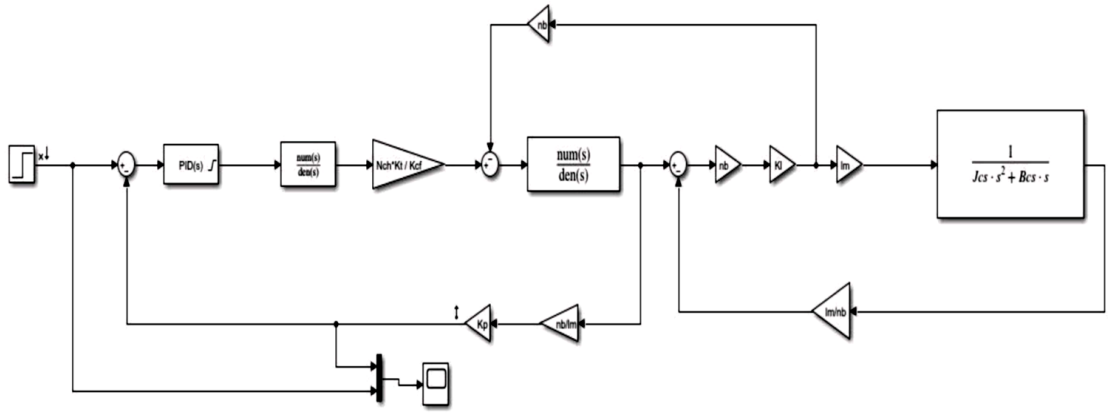

Fig.8 Simulink model of FTC system (linear model)

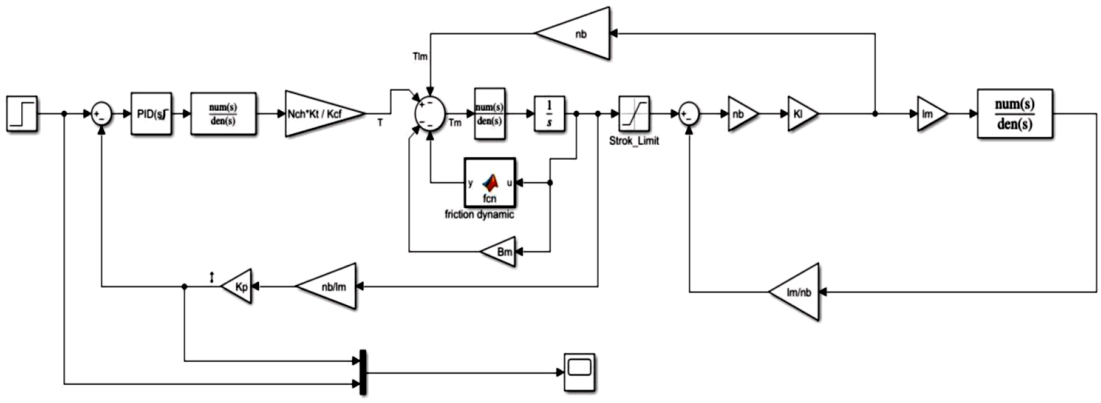

Fig.9 Simulink model of FTC system (non-linear model)

3.2. Performance Evaluation:

The step responses for Linear and Non-linear FTC model systems using the Simulink model are presented in Figures 10(a) and 10(b). The comparison between the two demonstrates the effectiveness of fault-tolerant control in handling diverse system dynamics. The Blue line represents the gain in both figures.

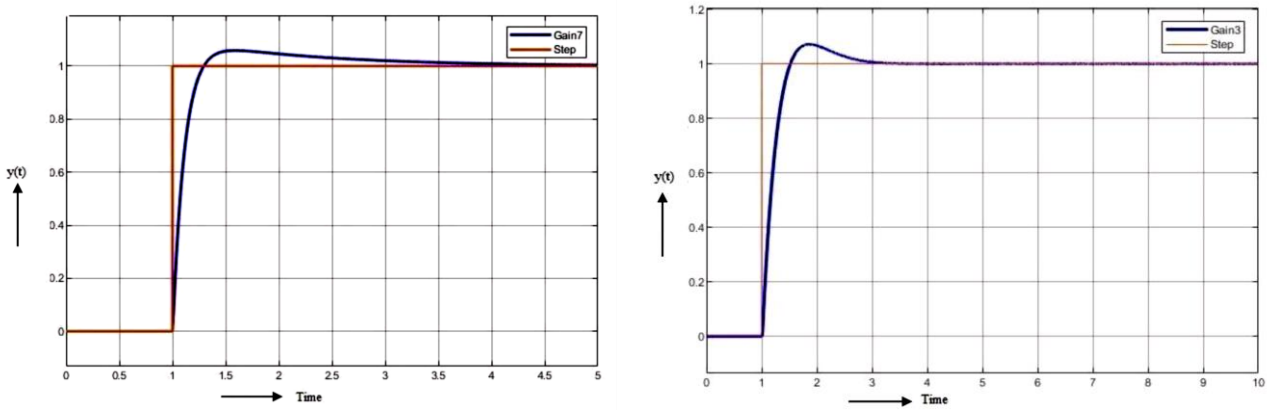

(a) FTC linear model system (b) FTC non-linear model system

Fig 10: Step Response of FTC System

The open-loop responses in Figures 11(a) and 11(b) highlight the inherent system dynamics without feedback intervention, while the closed-loop response in Figure 12 demonstrates the enhanced stability and control achieved through feedback. The frequency domain analysis using bode plot provides insights into the system's robustness and performance under varying operational conditions.

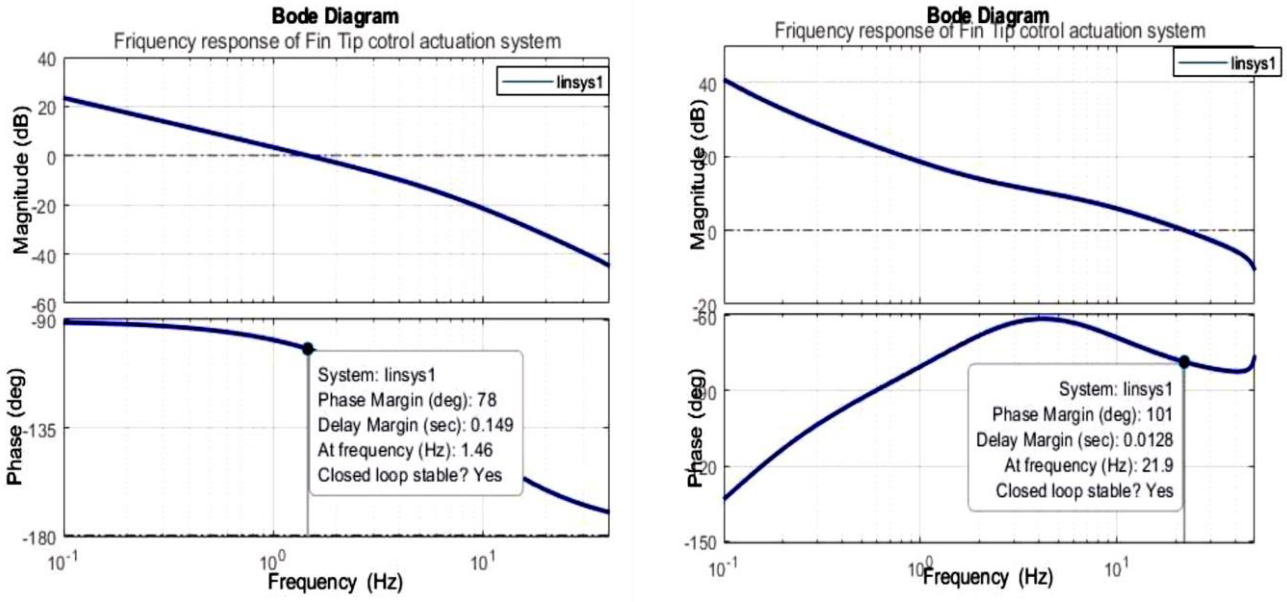

(a) FTC linear model system (b) FTC linear compensated system

Fig 11: Frequency Response of Open Loop FTC System

The gain margin and phase margin for these responses are outlined as follows:

- **Open-loop frequency response of the FTC linear model system:**

Gain margin: >80 dB

Phase margin: 78°

- **Open-loop frequency response of the compensated system (linear model):**

Gain margin: >80 dB
Phase margin: 101°

- **Closed-loop frequency response of the compensated system (linear model):**

Bandwidth: 17.7397 Hz
Specification for bandwidth: 17 ± 1 Hz
These results indicate a stable system with a sufficiently high phase margin and gain margin, meeting the specified bandwidth requirements for optimal performance.

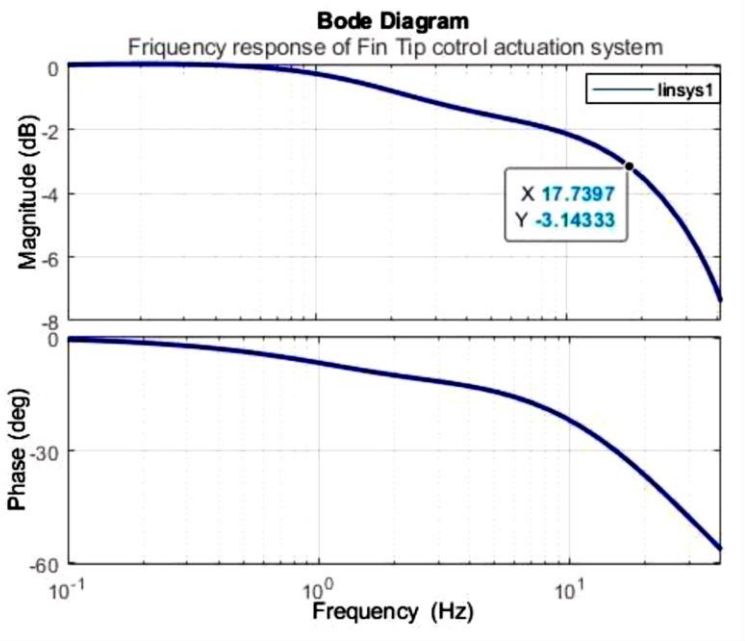

Fig 12: Frequency Response of Closed loop Compensated System (Linear Model)

The open-loop and closed-loop frequency responses provide additional confirmation of the system's stability and performance. Compensation strategies effectively address nonlinearities and dynamic complexities. The proposed FTC system achieves precise fin position control and satisfies the required performance criteria, as validated by simulations.

4. CONCLUSION

This study focuses on the servo system design, modelling, and simulation for Fin Tip Control (FTC) of a launch vehicle. It covers the mathematical modelling of the FTC, compensator design, and associated simulation results. The proposed FTC system uses electromechanical actuators, a PID controller, and a notch filter to achieve precise roll control. The simulation results indicate that the system meets the required performance specifications, ensuring stability and accuracy. The compensated system displayed robust gain and phase margins, showcasing its reliability. The closed-loop system's bandwidth aligned with the design specifications, highlighting the system's effectiveness in tracking and control.

Further improvements in control precision could be achieved by employing advanced friction compensation techniques, such as dynamic friction models that account for varying operating

conditions. There are numerous opportunities for advancing the efficiency and reliability of the launch vehicle's FTC servo system, future research could explore

- Implementation of advanced control methods, like adaptive control, which can adjust in real-time to varying system dynamics and uncertainties, improving the system's robustness.
- Development of fault-tolerant control systems to ensure system reliability despite component failures or unexpected disturbances.
- Incorporating machine learning methods to predict and compensate for nonlinear behaviours and un-modelled dynamics in the electromechanical actuation system could also offer significant benefits.
- Additionally, extensive real-world testing across diverse environmental conditions and thorough hardware-in-the-loop (HIL) simulations will be crucial for validating theoretical models and ensuring the practical effectiveness of the control strategies.

REFERENCES

[1]. Riyansh Sahu, Albert John Varghese, Rahul Satpute, SwatiVerma and Sudeep Kumar Sinha, “Simulation of Temperature Based Closed Loop Speed Control of BLDC Motor Using LabVIEW”, Advances and Applications in Mathematical Sciences, Volume 21, Issue 9, July 2022, Pages 5117-5124.

[2]. Albert John Varghese, Rejo Roy and S. R. Awasthi, "Intelligent Control Of Small VAWT Based WECS for Low Wind Speed Regions Using Advanced Hill Climb Search MPPT and BELBIC Controller", 2021 IEEE International Power and Renewable Energy Conference, Kollam, India, 2021, pp. 1-5, DOI: 10.1109/IPRECON52453.2021.9640873.

[3]. Albert John Varghese, Rejo Roy, and S Thirunavukkarasu, “Optimized Speed Control for BLDC Motor”, February 2014, International Journal of Innovative Research in Science Engineering and Technology, 2014, Volume 3, Special Issue 1, pp.1019-1030.

[4]. Albert John Varghese, Rejo Roy, and S. R. Awasthi, “Performance Evaluation of HAWT-and VAWT-Based WECS with Advanced Hill Climb Search MPPT and Fuzzy Logic Controller for Low Wind Speed Regions”, Smart and Intelligent Systems, 2021, pp. 97–113, DOI: 10.1007/978-981-16-2109-3_10.

[5]. Faustino J. Gomez and R. Miikkulainen, “Active guidance for a finless rocket using Neuro evolution”, Annual Conference on Genetic and Evolutionary Computation, 2023, pp. 2084-2095, DOI:10.1007/3-540-45110-2_105.

[6]. Laura Sopegno, Patrizia Livreri, Margareta Stefanovic and Kimon P. Valavanis, “Linear Quadratic Regulator: A Simple Thrust Vector Control System for Rockets”, 30th Mediterranean Conference on Control and Automation, Athens, Greece, 2022, pp. 591-597, DOI: 10.1109/MED54222.2022.9837125.

[7]. Du Wei, “Dynamic Modeling and Ascent Flight Control of Ares-I Crew Launch Vehicle”, Iowa State University, Ames, IA, USA, 2010.

[8]. David Bernacchia, “Design of Thrust Vectoring Attitude Control System for Lunar Lander Flying Testbed”, Graduation thesis in spacecraft attitude dynamics and control, Universita’ Di Bologna, 2020.

[9]. Dragan Lazic and Milan Ristanove, “M.R. Electro hydraulic thrust vector control of twin rocket engines with position feedback via angular transducers”, Control Engineering Practice, Vol. 15, Issue 5, 2007, pp.583-594, DOI:10.1016/j.conengprac.2006.10.015.

[10]. Bong Wie, Wei Du and Mark Whorton, “Analysis and design of launch vehicle flight control systems”, AIAA Guidance, Navigation and Control Conference and Exhibit, Honolulu, 2008, pp 18-21, pp. 6291,DOI: org/10.2514/6.2008-6291.

[11]. Emmanuel C. Agbaraji, Andrew Akwu, “Investigation on Controllability, Observability and Stability for Plant Optimal Control Performance”, European Journal of Engineering and Technology, Vol 4, Issue 4, 2016, pp.40-47.

[12]. Bhar Kisabo Aliyu, A. A. Funmilayo, Olusegun Samuel Sholiyi and Bhar Kisabo, “Pitch control of a rocket with a novel LQG/LTR control algorithm”, Journal of Aircraft and Spacecraft Technology, 2019, Vol 3, Issue 1, pp.24-37, DOI:10.3844/jastsp.2019.24.37.

[13]. Joao P. Hespanha, “Lecture notes on LQR/LQG controller design”, Knowledge Creation Diffusion Utililization, Vol 1, 2005, pp. 1-52.

[14]. Md. Rayid Hasan Mojumder, Naruttam Kumar, “PID, LQR, and LQG Controllers to Maintain the Stability of an AVR System at Varied Model Parameters”, 5th International Conference on Electrical Engineering and Information and Communication Technology, Dhaka, Bangladesh, 2021, pp 18-20, pp. 1-6.

[15]. Bhar Kisabo Aliyu, “Expendable Launch Vehicle Flight Control: Design & Simulation Matlab/Simulink”, Saint Petersburg State University of Aerospace Instrumentation, Russia, 2011, pp. 1-119.

[16]. E. A. Alandoli, M.Z.A. Rashid and Marizan Sulaiman, “A Comparison of PID and I-QR Controllers for Position Tracking and Vibration Suppression of Flexible Link Manipulator”, Journal of Theoretical and Applied Information Technology, 2017, Vol95, Issue 13, pp. 2949-2955.

[17]. Ahmed Wael and Quan Quan, “Robust hybrid control for ballistic missile longitudinal autopilot”, Chinese Journal of Aeronautics, 2011, Vol. 24, Issue 6, pp.777-788.

[18]. Chia-Ling Lee and Chao-Chung Peng, “Analytic Time Domain Specifications PID Controller Design for a Class of 2nd Order Linear Systems: A Genetic Algorithm Method”, IEEE Access, 2021, Vol9, pp. 99266-99275, DOI: 10.1109/ACCESS.2021.3093427.